Article published in Composites Part A-Applied Science And Manufacturing, vol. 66, Nov. 2014, pages 1-15.
DOI: 10.1016/j.compositesa.2014.06.019
web site: http://www.sciencedirect.com/science/article/pii/S1359835X14001985

Infiltrated Cu8Al-Ti alumina composites

C. Krüger[a,*], A. Mortensen[a]

[a]*Laboratory for Mechanical Metallurgy, Institute of Materials, École Polytechnique Fédérale de Lausanne, Station 12, CH - 1015 Lausanne, Switzerland*

Abstract

The effect of titanium additions on the interface and mechanical properties of infiltrated Cu8wt%Al-Al_2O_3 composites containing 57±2 vol% ceramic are investigated, exploring two different Al_2O_3 particle types and four different Ti concentrations (0, 0.2 ,1, 2 wt%Ti). Addition of 0.2wt%Ti leads to the development of a thin (5-10 nm) layer enriched in Ti at the interface between Cu alloy and Al_2O_3 particles; this Ti concentration produces the best mechanical properties. With higher Ti-contents $Ti_3(Cu,Al)_3O$ appears; this decreases both the interface and composite strength. Composites reinforced with vapour-grown polygonal alumina particles show superior mechanical properties compared to those reinforced by angular comminuted alumina particles, as has been previously documented for aluminium-based matrices. Micromechanical analysis shows that damage accumulation is more extensive, as is matrix hardening by dislocation emission during composite cooldown, in the present Cu8wt%Al matrix composites compared with similarly reinforced and processed Al-matrix composites.

Keywords: A. Metal-matrix composites (MMCs), A. Particle Reinforcement, B. Fibre/matrix bond, D. Mechanical testing

1. INTRODUCTION

There has been sustained interest over roughly the past 15 years in composites that combine copper with a ceramic reinforcement; this is because such materials have potential where high conductivity is to be coupled with high hardness, high wear resistance, or low thermal expansion. Pure or alloyed copper has thus been combined with ceramics as diverse as TiB_2 [1–7], Al_2O_3 [1, 8–11], several forms of carbon [12–16] or various carbides [17–21]; Ref. [22] gives a review of their processing methods and mechanical properties. Of the several pathways to their production, infiltration [23] is generally the method of choice when a high fraction of ceramic is desired.

One challenge in the processing of Cu-Al_2O_3 composites is posed by the fact that the interface between Cu and Al_2O_3 is often weak [24–26]. To bond copper with oxide ceramics such as alumina (be it in composite

*Corresponding author
Email addresses: krueger_carmen@web.de (C. Krüger), andreas.mortensen@epfl.ch (A. Mortensen)

processing or in brazing), elements that are interface-active and have a strong affinity for oxygen, notably Cr or Ti [25, 27, 28], are often added to copper. There are two interrelated reasons for this. The first has to do with wetting: these elements generally enhance wetting of oxides by molten copper. The second has to do with bonding: Cr and Ti tend to produce a stronger bond between copper and the ceramic. The two phenomena are indirectly related: a reduction of the wetting angle does not imply a stronger interface; however, both are favored by a higher work of adhesion W_a:

$W_a = \sigma_{LV} + \sigma_{SV} - \sigma_{SL} = \sigma_{LV} \cdot (1 + cos\theta)$

with σ_{SL}, σ_{SV} and σ_{LV} being, respectively, the interface energy between solid and liquid, solid and vapor, and liquid and vapor phase. θ is the wetting angle of the liquid on the solid.

If one adds Ti or Cr to copper, θ is significantly reduced; however the underlying mechanisms are different. Chromium affects oxygen adsorption to the metal-Al_2O_3 interface and as such reduces σ_{SL}, in turn lowering the wetting angle of liquid copper on alumina. Titanium in copper reduces alumina and leads to the formation of titanium oxides [24, 29–31] and/or mixed Cu-Ti oxides [32–34] along the interface. Detailed investigations of the interface between Cu-Ti alloys and Al_2O_3 show that two phases generally appear between the metal and the ceramic [35–37], reducing θ drastically to a value below 90°[24, 28, 29, 38, 39]. The formation of these phases smoothens the transition between metallically bonded copper and ionocovalently bonded alumina, causing in general a reduction in the wetting angle and an increase in the work of adhesion, this tending in turn to increase the mechanical strength of the interface. This effect is exploited in commercially available Cu or Cu-Ag brazes designed to bond ceramics. These typically contain Ti additions [34, 40]; their wetting and interfacial reactivity have been studied in detail in Refs. [28, 35–37]. Nicholas et al. [38] documented the influence of third elements on the wetting of Cu-Ti alloys on Al_2O_3, to conclude that the addition of up to 30 at% aluminum influences only slightly the Cu-Ti alloy wetting angle. Additionally, oxygen is known to influence wetting in copper alloys containing elements with a high affinity to oxygen; data and the underlying physics are reviewed in References [25, 26].

We study here the influence of a varying Ti content (0 to 2 wt%) in a Cu8wt%Al alloy on the structure and properties of alumina reinforced composites produced by pressure infiltration. Our main goal in exploring these additions is to tailor the interfacial strength, aiming to produce strong, non-brittle, alumina particle reinforced copper for applications requiring a high fraction of ceramic in the composite.

2. EXPERIMENTAL PROCEDURES

Cu-8wt%Al (Cu8Al), Cu-8wt%Al-0.2wt%Ti (Cu8Al0.2Ti), Cu-8wt%Al-1wt%Ti (Cu8Al1Ti) and Cu-8wt%Al-2wt%Ti (Cu8Al2Ti) alloys were produced and cast in a high-vacuum induction furnace under Ar atmosphere in Al_2O_3 crucibles. Starting materials were Cu (4N), Al (4N) and a Cu-28wt%Ti alloy more than 99,5% pure. The use of Ti in the alloys always led to formation of a thin reaction layer along the surface of the Al_2O_3

crucibles, so that the true Ti-content in the alloys is slightly lower than the nominal values given here.

The particles used for production of the composites are (i) α-Al_2O_3 F320 (purity 99.5%, main impurity Na) purchased from Treibacher Schleifmittel (Germany), obtained by fusion of Bayer alumina, followed by comminution and (ii) AA 18 (purity 99.99%) from Sumitomo (Japan), produced by in-situ chemical vapor deposition [41]. Their mean diameter $D_{V,0.5}$, measured by laser diffraction in a Mastersizer (Malvern Instruments, United Kingdom), is 36 μm and 22 μm, respectively.

Preforms of both powders were packed and then densified by tapping and mechanical vibration, directly within the Al_2O_3-crucibles. A metal ingot was then placed on top of the preform into the crucible. Heating in the pressure-infiltration apparatus was started once a stable primary vacuum was reached (a detailed description of the apparatus is given in Ref[42]). Complete infiltration of the preform with liquid metal was obtained with an applied gas pressure of 8 MPa held for 3 minutes at 1150±10°C.

Samples for testing were produced from the infiltrated ingots by electro discharge machining. A few machined samples from each composite ingot were exposed to a high temperature heat treatment to check whether this brings alterations in phases present, the interface structure, or composite properties. The heat treatment consisted in a hold at 800°C during 8 h followed by slow furnace cooling. For simplicity the composites are hereafter named according to their composition, e.g. Cu8Al1Ti-AA18 is a composite of AA18-Al_2O_3 particles within a Cu8Al1Ti matrix, and HT indicates that the heat treatment was applied.

For microstructural characterization, sample sections were polished and observed by Scanning Electron Microscopy (SEM) on a FEI XLF30 equipped with Energy-Dispersive X-ray spectroscopy (EDX) (FEI, USA). The particle morphology after infiltration was investigated by SEM after electrolytic deep etching of the matrix with etchant D2 by Struers (Denmark). Two specimens for Transmission Electron Microscopy (TEM) were prepared with a focused ion beam (FIB) instrument equipped with a dual ion/electron beam (Zeiss, Germany). The TEM lamellae were observed in a Tecnai Osiris (200 kV, 2 nA, FEI, USA) equipped with an EDX detector. For X-Ray Diffraction (XRD) of the infiltrated powders, the metallic matrix was dissolved in nitric acid (38%); the diffractometer used is a D8 from Bruker (Germany) with a Cu-Kα radiation source.

The volume fraction of particles in the composites was determined by densitometry using a Sartorius MCP 210P (IG Instrumenten-Gesellschaft, Switzerland) microbalance and its YDK 0.1 gravity determination kit, assuming full infiltration (this being justified by the absence of pores in the microstructure). Vickers Hardness was measured with a load of 20 kgf held for 16s. Young's Modulus E was evaluated by measuring the ultrasonic resonance frequency on a Grindosonic (Lemmens N.V., Belgium) using cylindrical bars of composite with a diameter of 5 mm and a length of 50 mm, cut longitudinally from the as-cast billets by electrical discharge machining. The ASTM E1876 [43] standard was used for calculation of Young's modulus assuming a Poisson's ratio of ν=0.3 for all composites. This calculation of Young's modulus is not very sensitive to the value of Poisson's ratio: the maximum relative variation is by 1% if ν is varied from 0.24 to 0.34, these being

values for Al_2O_3 [44] and pure Cu [45], respectively.

Tensile tests were conducted at a nominal strain rate of 10^{-4}/s on a MTS (USA) RT50 universal tensile testing machine equipped with a double-sided extensometer (Mini MFA 2, MF, Germany). Compression tests were conducted on a Schenck TREBEL (Germany) at the same strain rate. The tensile specimens were undersized dogbone samples, of geometry according to the ASTM E-8M [46] standard, with a reduced section length of 25 mm, a width of 6 mm and a thickness of 2 mm. The compression test specimens were cylinders of round section with a diameter of 3 mm and a height of 6 mm. Where multiple tests were conducted on similar samples, values and error bars given for hardness values, tensile and compression data are averages and standard deviations, respectively.

3. RESULTS

3.1. Microstructure and characterization of interface

SEM images of the virgin Al_2O_3 powders are given in Fig.1. The AA18 particles are nearly equiaxed with some facets and no immediately apparent defects along their surface. The F320 particles are angular, have higher aspect ratios and show surface cracks. Diffraction patterns of the initial Al_2O_3 powders are shown in Fig.2. While AA18 is composed only of α-Al_2O_3, there are two phases present in F320: (i) α-Al_2O_3 and (ii) the so-called β-Al_2O_3 [47], an alumina variant that is stabilized by the presence of Na_2O: $Na_2O{\cdot}11Al_2O_3$ and formed during the classical Bayer process.

The alloys used for production of the composites were examined for the presence of second phases. Cu8Al is a single-phased α-Cu(Al) solid solution, while all alloys containing Ti have a second phase, which is visible in Fig.3. Its volume fraction increases with increasing Ti content in the matrix. The diffractogram given by this phase after dissolution of the α-Cu(Al) phase from a sample of 100% matrix shows the second phase to be $AlCu_2Ti$[48].

Composite microstructures are shown in Fig.4. The composites are completely infiltrated and defect-free. In composites with Ti-containing matrices, a third phase is visible, mainly at the ceramic-metal interface, Fig.5.

The structure of the interface can be seen more in detail in Fig.6, where the polycrystalline nature of the interface phase covering the alumina can be distinguished after electrolytic deep-etching of the matrix. One can also see on this figure a branched secondary phase structure emerging out of a larger zone of metal devoid of alumina particles.

How the presence and structure of the interface phase evolves with titanium content is shown in Fig.7, where an electrolytically etched microstructure of each composite is shown. The volume fraction of the interface phase increases with increasing titanium content, from a few patches along the interface in Cu8Al0.2Ti matrix composites to a continuous layer covering practically all particles when the matrix is Cu8Al2Ti.

The composition of this interfacial phase was determined by XRD characterization of powders extracted by

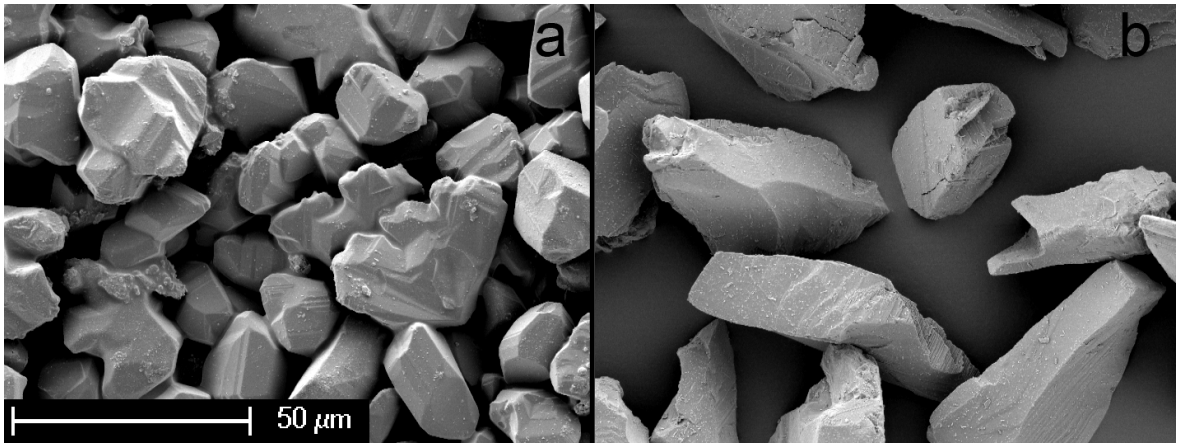

Figure 1: Al_2O_3 powders, a: AA18 and b: F320

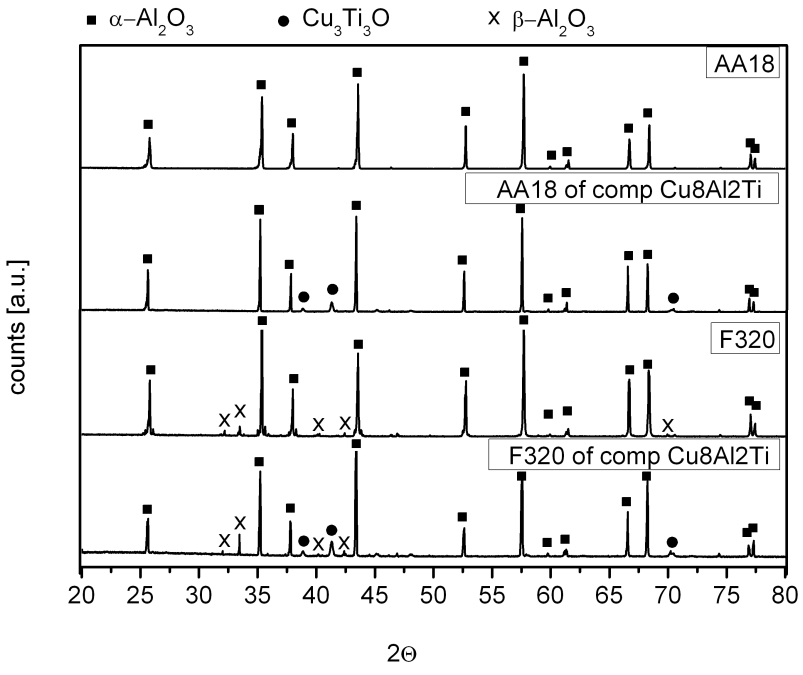

Figure 2: XRD Diffraction patterns of Al_2O_3 particles, of both types respectively in virgin state and as leached from a composite with a matrix of Cu8Al2Ti

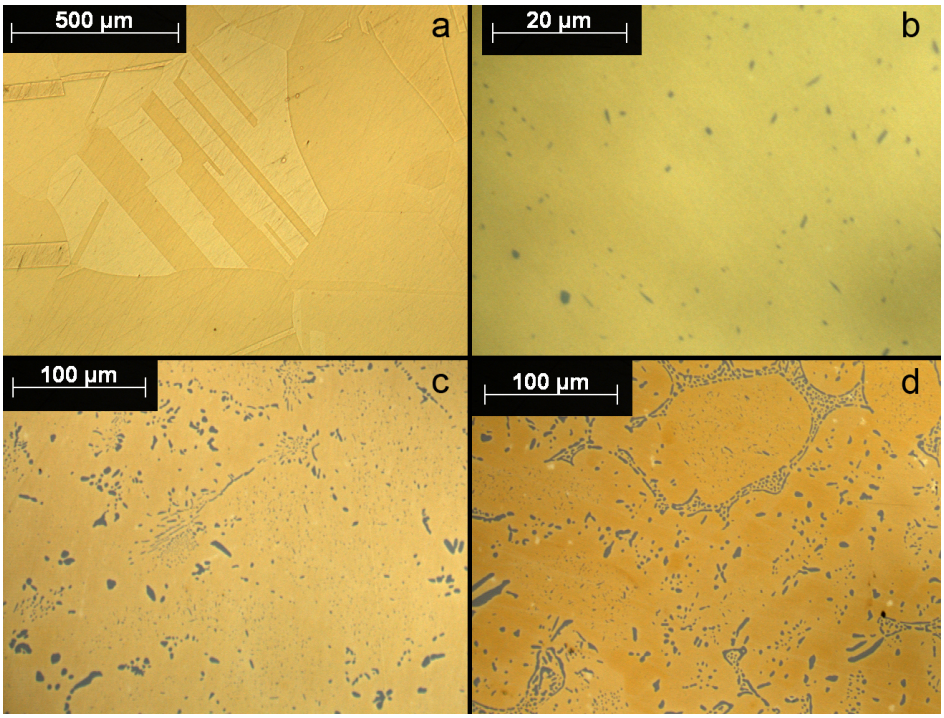

Figure 3: Light microscopy images of a: Cu8Al, b: Cu8Al0.2Ti, c: Cu8Al1Ti and d: TiCu8Al2Ti all after heat treatment

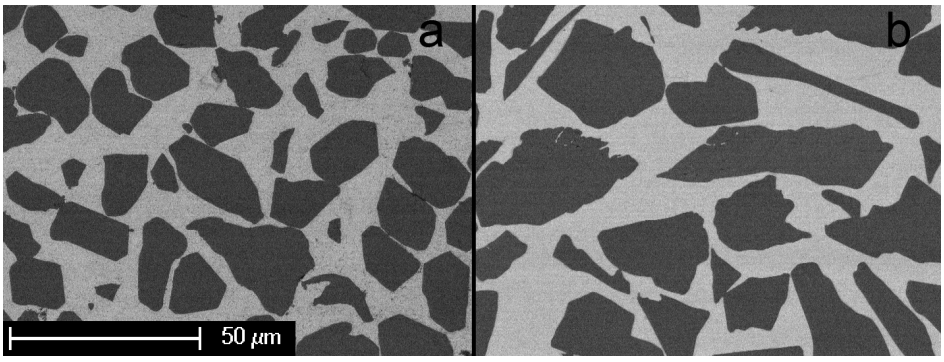

Figure 4: Backscattered electron SEM image showing microstructure of a: Cu8Al-AA18 and b: Cu8Al2Ti-F320

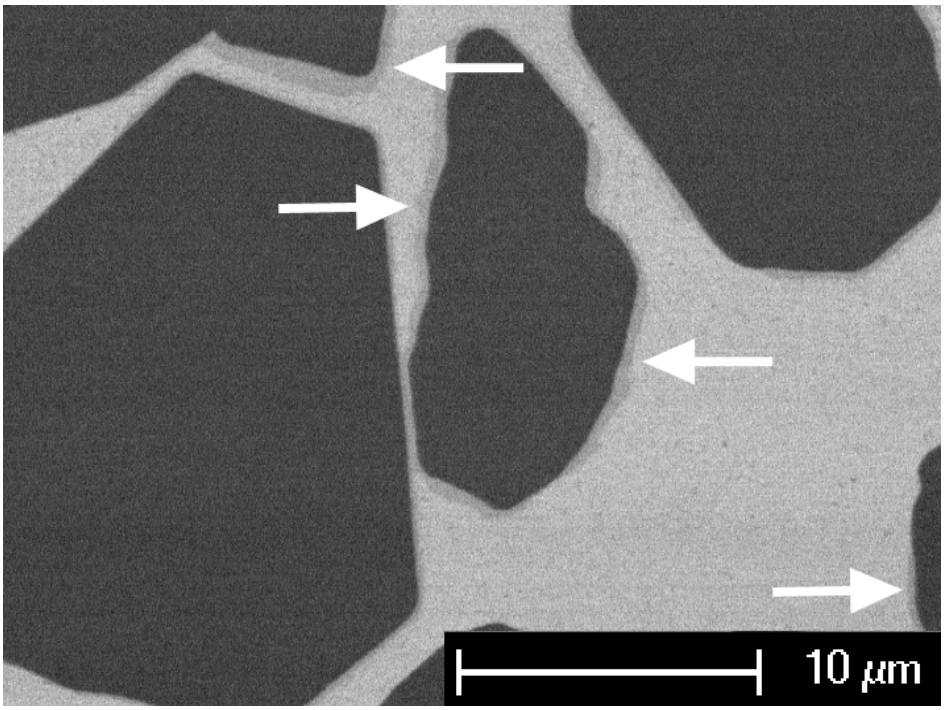

Figure 5: Backscattered electron SEM image revealing a third phase present at the interface between ceramic and metal in Cu8Al2Ti-AA18

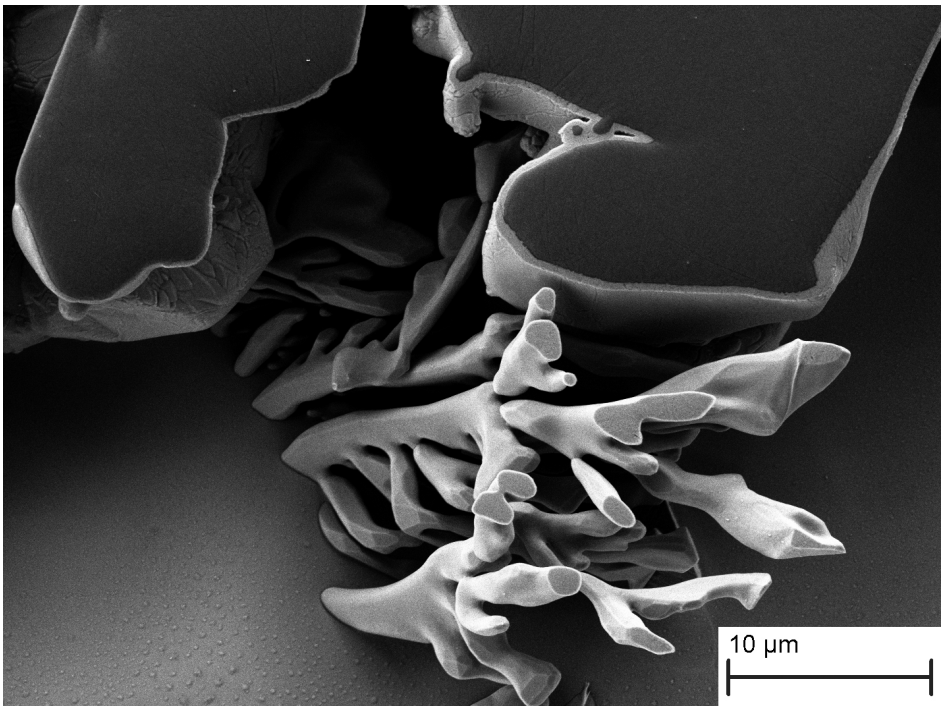

Figure 6: SEM image after electrolytic etching, revealing both the phase present at the interface between ceramic and metal as well as a branched secondary phase in the matrix of Cu8Al2Ti-AA18

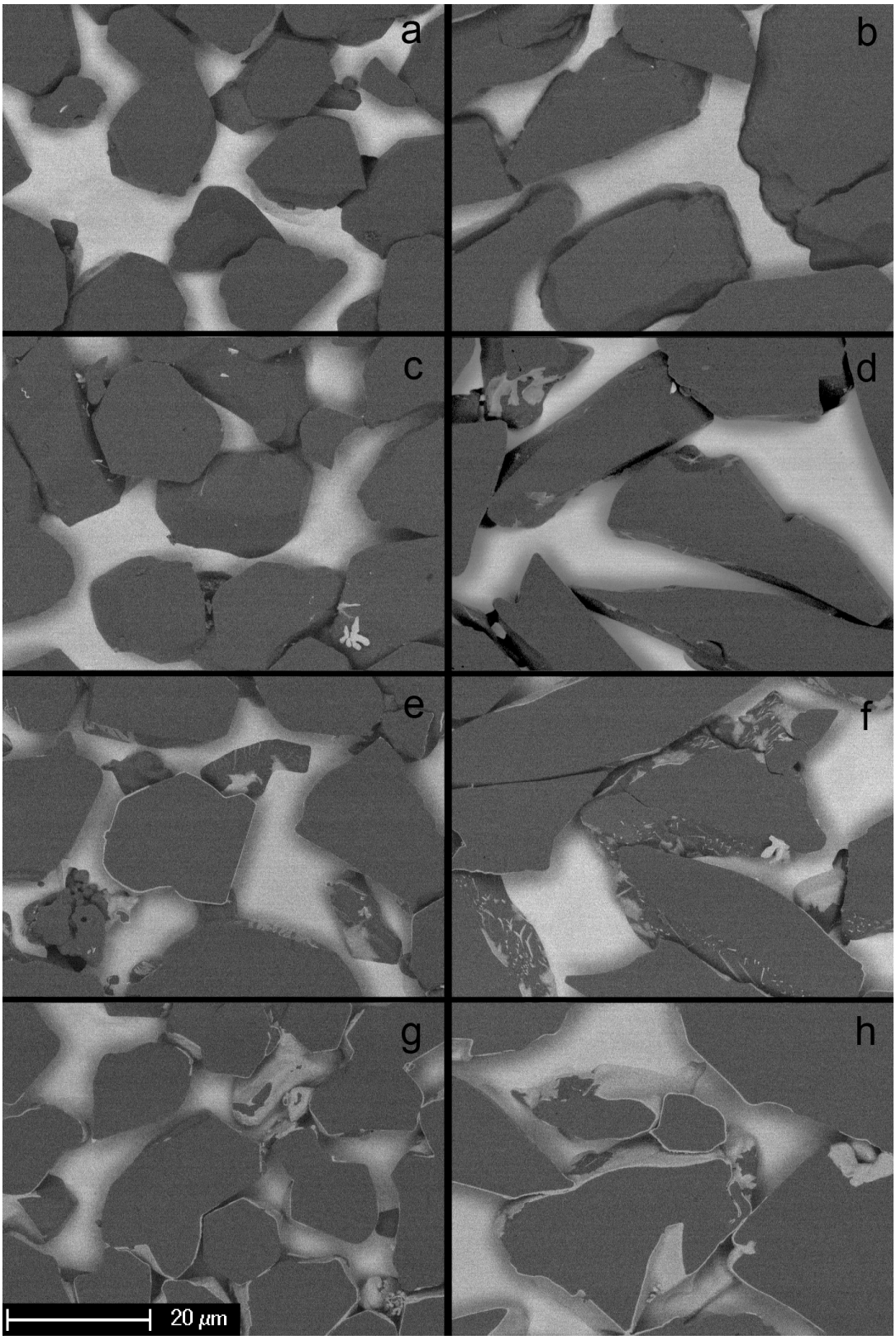

Figure 7: Backscattered SEM-images of particles (dark) and matrix (white) after electropolishing of a: Cu8Al-AA18, b: Cu8Al-F320, c: Cu8Al0.2Ti-AA18, d: Cu8Al0.2Ti-F320, e: Cu8Al1Ti-AA18, f: Cu8Al1Ti-F320, g: Cu8Al2Ti-AA18 and h: Cu8Al2Ti-F320, revealing in addition the presence of interfacial second phases (light grey)

full dissolution of the matrix phase, see Fig.2: it is a ternary Cu-Al-Ti oxide. Its exact lattice parameters were deduced by Rietveld-refinement of the diffraction patterns; the result is 11.346 Å on AA18 and 11.344 Å on F320 particles. This leads to identify the interface phase by comparison with Kelkar et al. [49] to be Ti_3Cu_3O with Al replacing some Cu atoms on the Wyckoff c-positions in the lattice i.e. $Ti_3(Cu,Al)_3O$.

In addition to this phase, there are also small but detectable peaks of $AlCu_2Ti$ present in diffractograms of all powders after leaching of Ti-containing matrices. One also can estimate from these SEM images that there is a branched phase present, seemingly distinct from Ti_3Cu_3O (see lower right-hand corner of Fig.7c), which does not show a branched structure. The branched structure appearing in Fig.6 is therefore probably a product of solidification of the alloy, most likely $AlCu_2Ti$ (while the phase covering the alumina particles is $Ti_3(Cu,Al)_3O$).

Further characterization of the interface was carried out by producing an electron-transparent section of the interface between Al_2O_3 and the primary copper-rich alloy phase along a region of the interface devoid of the mixed $Ti_3(Cu,Al)_3O$ oxide in a Cu8Al0.2Ti-AA18 composite, see Fig.8a. Along a line through the interface in this section, elemental EDX-mapping was performed. As shown in Fig.8, there is a continuous layer at the interface between the matrix (dark phase) and the alumina particles (bright phase). According to the results of elemental mapping, shown in Figs.8b to 8f, this 5-10 nm thick layer is rich in titanium and contains smooth gradients in the concentration of other elements (O, Cu and Al, all three of which vary more smoothly than does the Ti concentration, suggesting that these do not vary according to a step function). A similar TEM result was obtained at a similar (but rarer, given the nearly continuous mixed oxide layer) location in a composite CuAl2Ti-AA18 composite.

The limited scope of TEM characterization of this interface in the present investigation precludes concluding whether the increased Ti content along the interface between alumina particles and the alloy primary phase corresponds simply to an increased concentration of Ti in one or both of the metal or the ceramic phases along the interface, or to the formation of a very thin but distinct layer of a separate phase. In any event, present data establish unambiguously that titanium also alters the interface between Al_2O_3 and the copper-rich alpha phase in regions that are free of the thicker, clearly visible interfacial ternary Cu-Al-Ti oxide.

3.2. Mechanical properties

An overview of mechanical properties measured on the composites is given in Table 1.

Young's modulus E is higher for AA18 composites and it decreases slightly with increasing Ti content. In F320 composites E increases with increasing matrix Ti content. As also shown in Table 1, the density of the AA18 composites is slightly lower than for the F320 composites but does not vary significantly with the matrix Ti content. From the density of composites having a Cu8Al matrix without Ti addition (which leads to the formation of new phases and thus falsifies the result somewhat), we determine the volume fraction of Al_2O_3 particles to be 0.59 for AA18 particles and 0.56 for F320 particles.

The hardness of composites containing AA18 alumina is higher than that of composites based on F320 alumina.

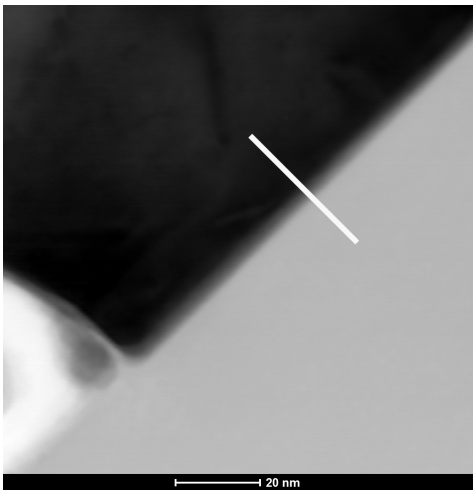

(a)

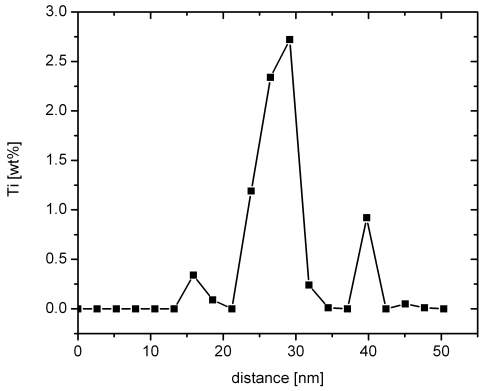

(b)

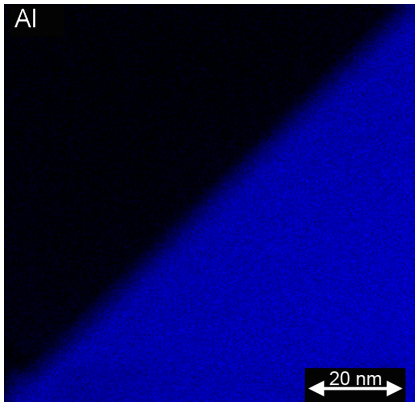

(c)

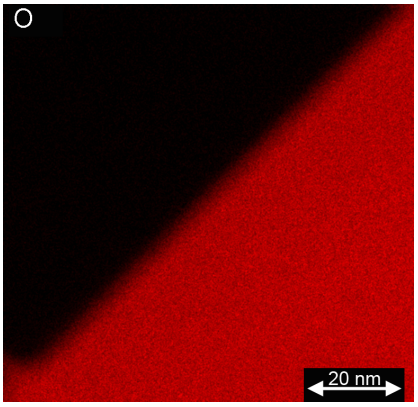

(d)

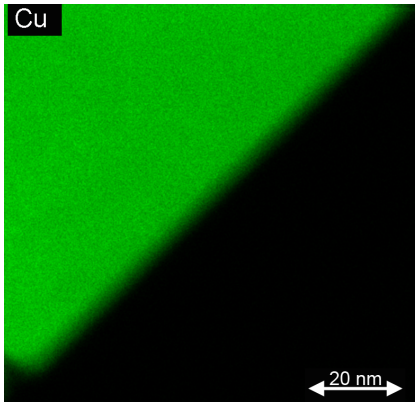

(e)

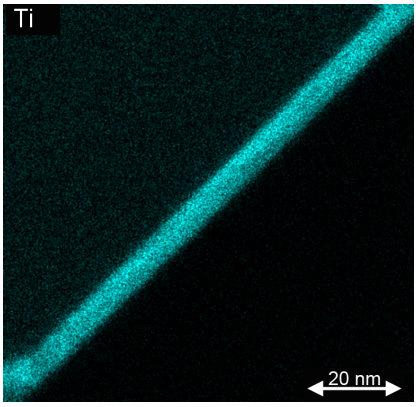

(f)

Figure 8: (a) TEM bright field image of Cu8Al0.2Ti-AA18 of area where EDX-mapping and line-scan, indicated by the white line, is performed (b) elemental distribution in line-scan (c) Al distribution (d) O distribution (e) Cu distribution (f) Ti distribution

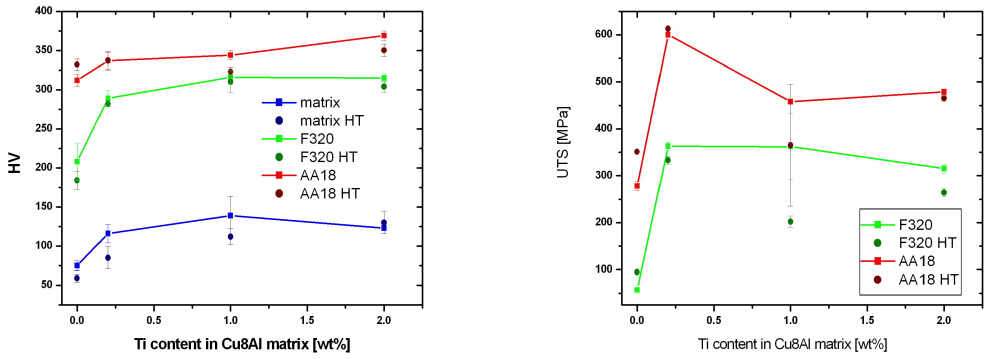

(a) (b)

Figure 9: Evolution with titanium content of composite properties (a) Hardness of infiltrated composites and matrices (b) UTS of infiltrated composites

Table 1: Mechanical properties of the composites

composite	E [GPa]	density [g/cm^3]	HV10	UTS [MPa]	ϵ [%]	$\sigma_{0.2\%}$
Cu8Al-AA18	240-248	5.5	312±8	332±7	0.2	476±35
Cu8Al0.2Ti-AA18	232-242	5.5	337±11	600±5	1.0-1.1	597±7
Cu8Al1Ti-AA18	226-232	5.5	344±6	409±75	0.3-0.5	624±11
Cu8Al2Ti-AA18	229-243	5.5	369±6	479±6	0.4	627±4
Cu8Al-F320	151-158	5.6	208±24	57±1	0.2-0.3	181±34
Cu8Al0.2Ti-F320	176-182	5.6	289±10	363±8	0.5-0.7	461±10
Cu8Al1Ti-F320	199-204	5.6	316±9	281±71	0.2-0.4	518±7
Cu8Al2Ti-F320	210-215	5.6	315±6	315±10	0.3	539±20

The hardness of both composites and matrices is increased by addition of 0.2wt%Ti but further addition of Ti to the matrix does not lead to much further hardening, Fig.9a. The heat treatment lowers the hardness of the matrices, but does not do so markedly for the composites.

In tensile tests, Ultimate Tensile Strength (UTS) values measured at the maximum in the curves were obtained for Cu8Al0.2Ti-AA18 composites, see Fig.10 and Table 1: 600 MPa with an elongation of one percent. Again, AA18 composites are superior to F320 composites having the same matrix, regardless of its composition. The most performant F320 composite has a matrix of Cu8Al0.2Ti and shows a UTS of 363 MPa with a tensile elongation of 0.6%, see Table 1. The large error bars (and hence spread in measured values) for composites with a Cu8Al1Ti matrix may signal the presence of internal defects (bands of matrix devoid of particles, often called veins) in some of those samples. Composites with a Cu8Al2Ti matrix show lower UTS and elongation: 480 MPa and 0.4% for Cu8Al2Ti-AA18 and 320 MPa and 0.3% for Cu8Al2Ti-F320. The

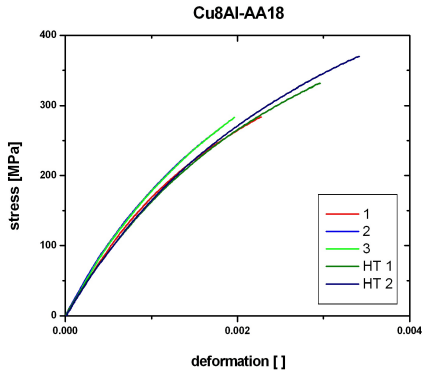

(a)

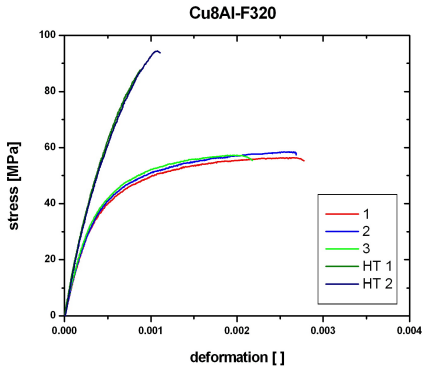

(b)

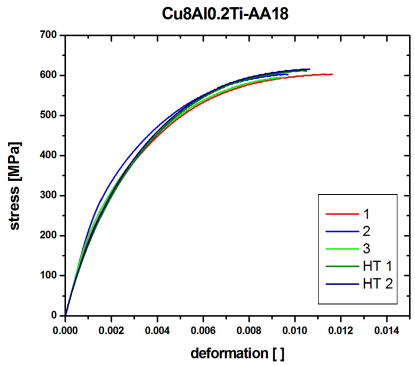

(c)

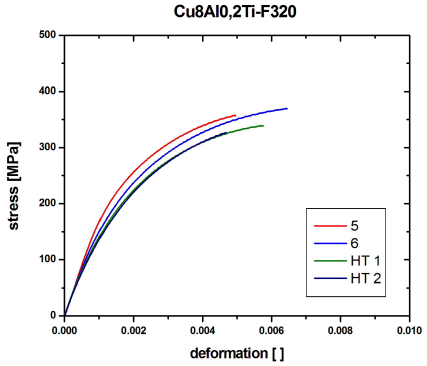

(d)

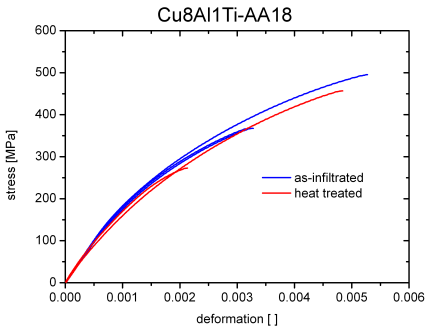

(e)

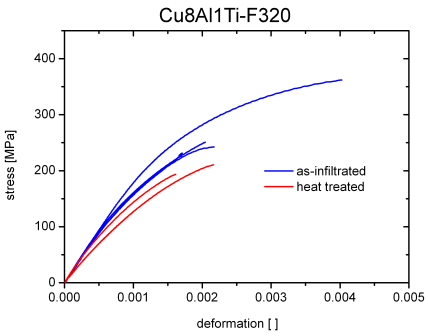

(f)

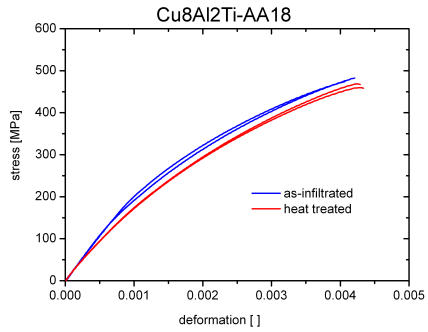

(g)

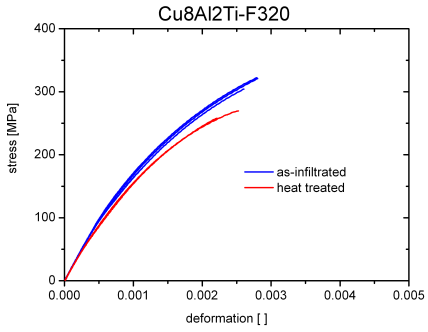

(h)

Figure 10: Tensile curves of infiltrated composites: (a) Cu8Al-AA18 (b) Cu8Al-F320 (c) Cu8Al0.2Ti-AA18 (d) Cu8Al0.2Ti-F320 (e) Cu8Al1Ti-AA18 (f) Cu8Al1Ti-F320 (g) Cu8Al2Ti-AA18 (h) Cu8Al2Ti-F320

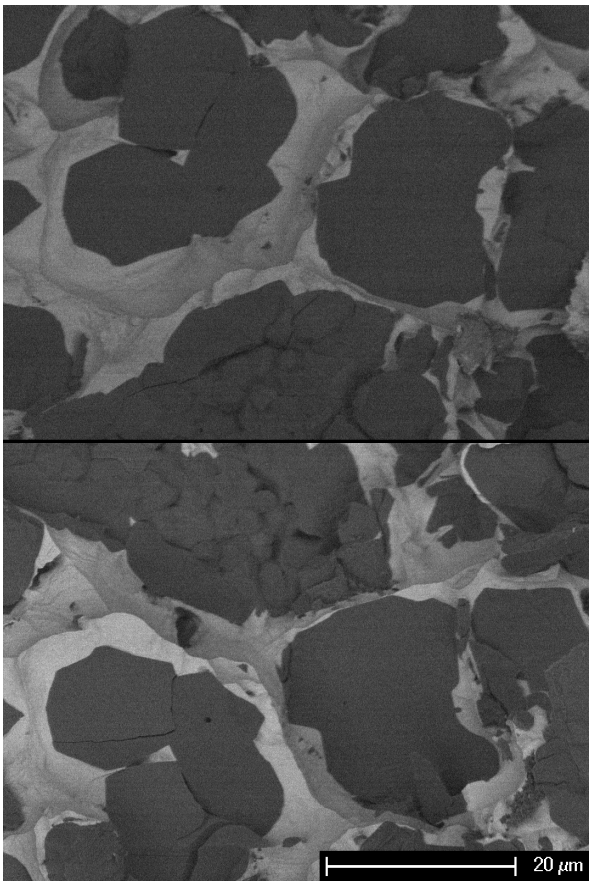

Figure 11: Backscattered electron SEM image: matching fracture surfaces of Cu8Al0.2Ti-AA18

least performant composites are those having a titanium-free Cu8Al matrix; heat treatment slightly improves their properties. For Cu8Al-AA18 the UTS reaches 280 MPa and 0.2% elongation without heat treatment and 330-370 MPa and 0.3% after heat treatment, see also Fig10a. The heat treatment almost doubles the UTS for Cu8Al-F320: from 60 MPa to 95 MPa, but the absolute value still remains very low. Elongation is concomitantly reduced from 0.2-0.3% to 0.1%, see Fig.10b, these too being very low values. The heat treatment shows no noticeable influence on the tensile properties of composites with a matrix other than Cu8Al.

Fracture surfaces of the strongest and most ductile material, Cu8Al0.2Ti-AA18, reveal broken particles. These are evidenced by the presence of the same (broken) particle on both sides of the fracture surface, see Fig.11. For comparison, we also show the corresponding fracture surfaces of the least ductile material Cu8Al-F320: here, one does not observe cracked particles but rather traces of Al_2O_3 particles that were taken out by decohesion from the matrix, see Fig.12. The fracture surfaces of Cu8Al1Ti-AA18 in Fig.13 and the polished cross-section along a tensile specimen of Cu8Al2Ti-AA18, shown in Fig.14, also reveal broken alumina particles after tensile fracture of both materials; however, in both the interface phase also undergoes brittle fracture.

We measured the evolution of Young's modulus with increasing strain in samples of Cu8Al0.2Ti-AA18 and

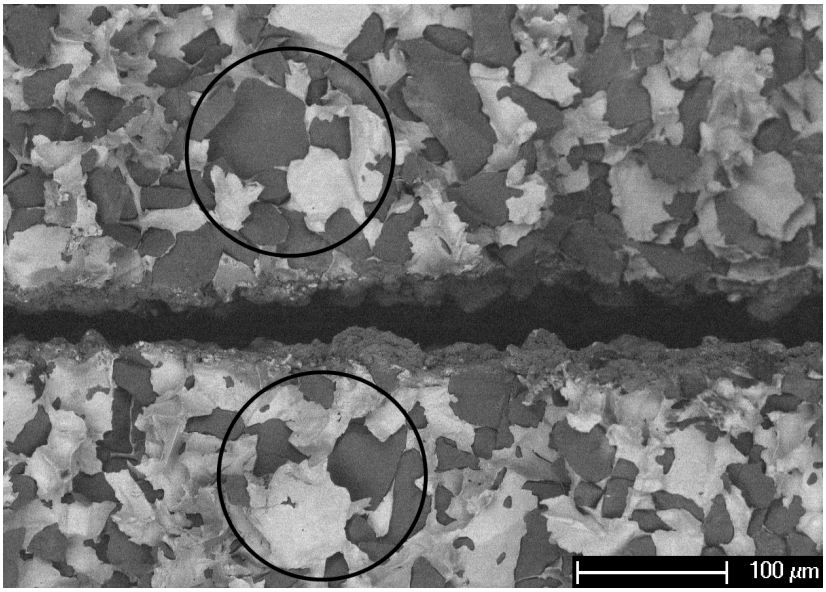

Figure 12: Backscattered electron SEM image: matching fracture surfaces of Cu8Al-F320

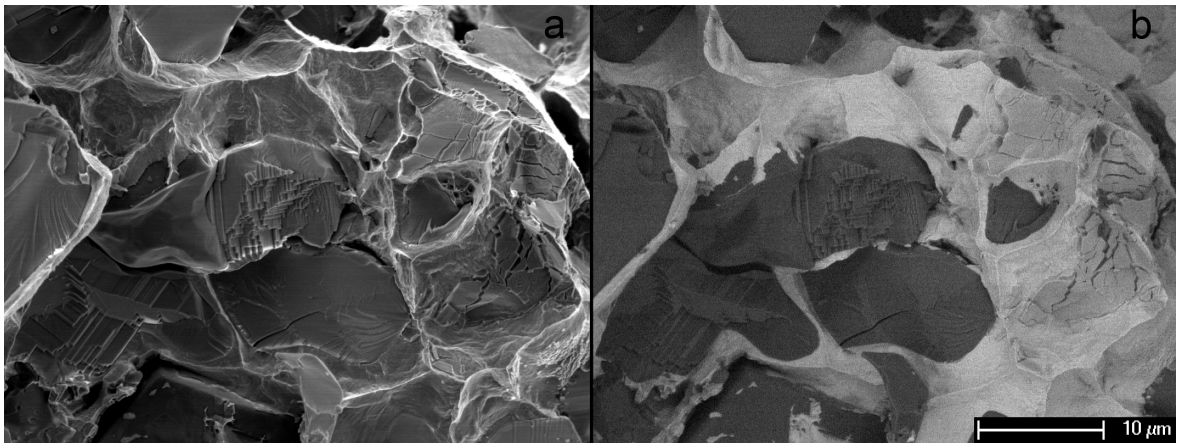

Figure 13: Fracture surface of Cu8Al1Ti-AA18 a: SE image, b: Back-Scattered Electron (BSE) image

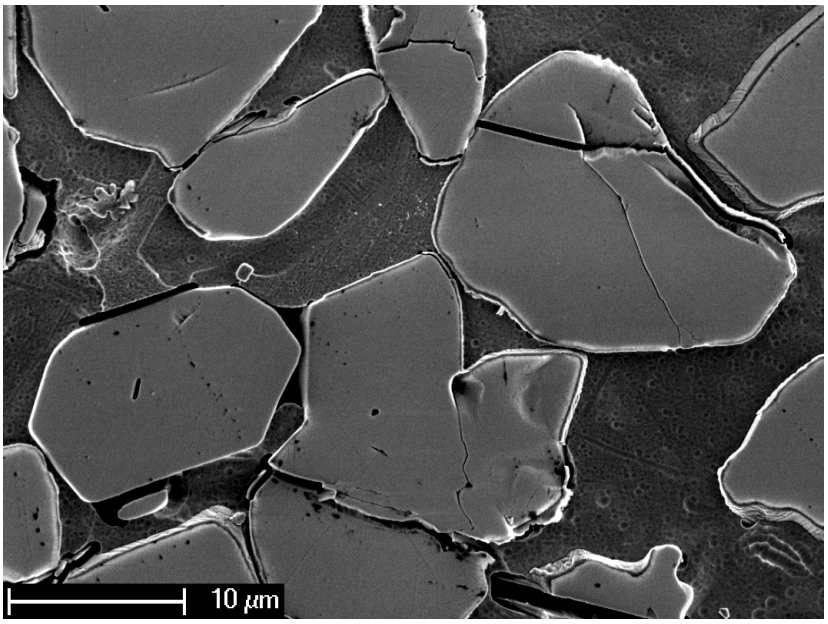

Figure 14: SEM image of longitudinal cross-section of tensile specimen of Cu8Al2Ti-AA18 polished and electrolytically etched, loading direction perpendicular to the scale bar

Cu8Al0.2Ti-F320, the most performant composites for both powder types. These were subjected to tensile tests with periodic cyclic unloading/reloading: at least eight unload-reload cycles were performed with an average stress of 50% and an amplitude of 40% of the maximal stress reached before unloading for each of a series of strain increments. The procedure is described in detail in Ref.[50] for similar aluminum-matrix composites. Generally, the slope of the curves needed two cycles to stabilize to a constant value, so that only the last four cycles during unloading were used for determination of Young's modulus. The initial Young's modulus E_0 was also determined by cycling within the initial elastic region. From these experiments, we determine the damage parameter D_E, defined as:

$$D_E = 1 - \frac{E}{E_0}. \tag{1}$$

D_E is plotted versus applied plastic strain in Fig.15a for Cu8Al0.2Ti-AA18 and in Fig.15b for Cu8Al0.2Ti-F320. Two composites were tested for each plot; as seen the data are quite reproducible. A linear fit yields the slope for D_E as a function of plastic strain to be 18 for Cu8Al0.2Ti-AA18 and 23 for Cu8Al0.2Ti-F320.

Room temperature compression test data are shown in Fig.16 as true stress-true strain curves corrected for sample surface roughness, i.e. the very beginning of the curves are replaced by linear fits prolonging the linear elastic region to zero stress. AA18 composites show higher compressive strength than do F320 composites. With increasing Ti content, the peak stress increases. The heat treatment does not influence the compressive behavior of the composites. The compressive 0.2% offset yield stress, $\sigma_{0.2\%}$, is given in Table 1. AA18 composites show higher $\sigma_{0.2\%}$ than F320 composites. For all composites and matrices, $\sigma_{0.2\%}$ increases with Ti

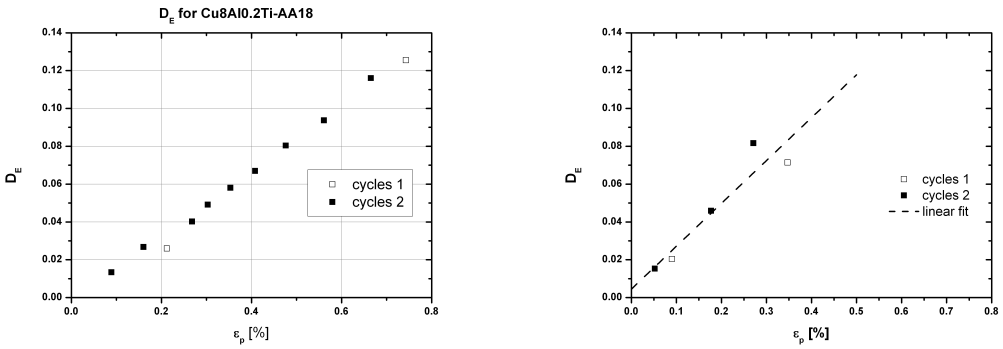

(a) (b)

Figure 15: Damage parameter D_E versus tensile plastic strain, as measured using periodic unloading of (a) two samples of Cu8Al0.2Ti-AA18 (b) two samples of Cu8Al0.2Ti-F320

content in the matrix.

4. DISCUSSION

4.1. Interface

Adding titanium to the matrix clearly alters the interface. With increasing Ti content, an increasing fraction of the alumina particle surface is covered with Ti_3Cu_3O containing some Al in solution. A second very thin layer rich in Ti was identified by TEM at a location where this mixed oxide $Ti_3(Cu,Al)_3O$ was absent along the interface between CuAl0.2Ti (or CuAl2Ti) and Al_2O_3, Fig.8.

The best tensile properties were measured for composites with Cu8Al0.2Ti alloys, which show only sparse coverage of the interface with $Ti_3(Cu,Al)_3O$. This implies that:

(i) the interface is mechanically strengthened by the 5-10 nm thick titanium-rich layer shown in Fig. 8 since composites with a matrix of Cu8Al0.2Ti have clearly stronger interfaces than titanium-free Cu8Al matrix composites;

(ii) the ternary oxide $Ti_3(Cu,Al)_3O$ is, on the other hand, detrimental, since cracks propagate through this phase, Fig.13 and Fig.14, and since increasing the proportion of the interface that it covers leads to lowered composite strength, Table 1, Fig.9b, Fig.10 and Fig.16.

Data exist in the literature on interfaces in systems that resemble the present metal/ceramic combination, namely CuTi-[28] or CuAgTi alloy [35–37, 51, 52] brazing or wetting experiments on Al_2O_3. Two layers were found: a first thin (200 to 1000 nm thick) layer of binary titanium oxide (of variable stoechiometry) followed, if the titanium content is above a value on the order of 1%, by an additional $Ti_3(CuAl)_3O$ layer a few micrometers thick, located between the titanium oxide and the metal.

The thickness of the interfacial layers in the present composites is much smaller compared to results from brazing or wetting experiments. This can first be related to the difference between the time during which the liquid

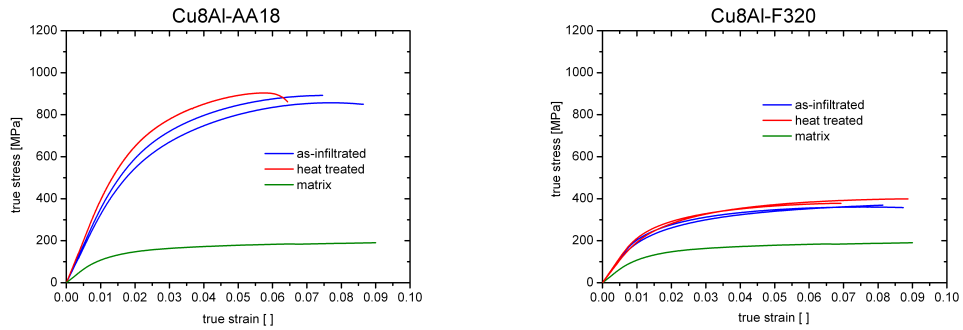

(a)

(b)

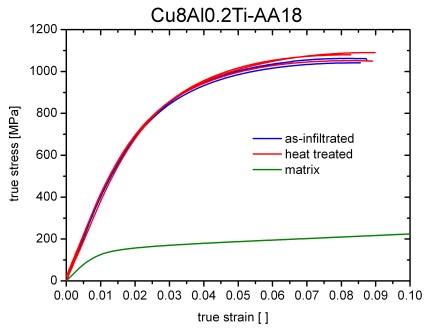

(c)

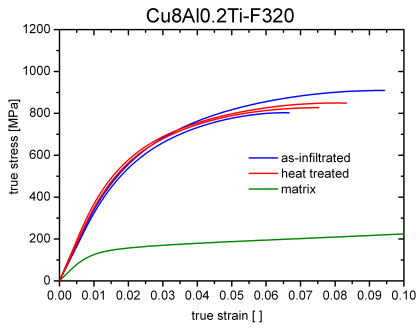

(d)

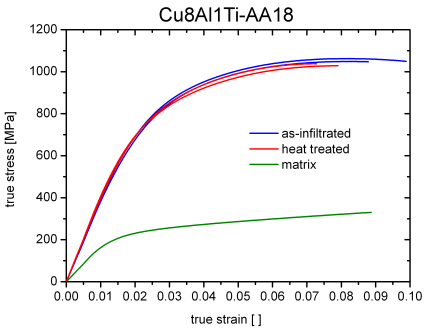

(e)

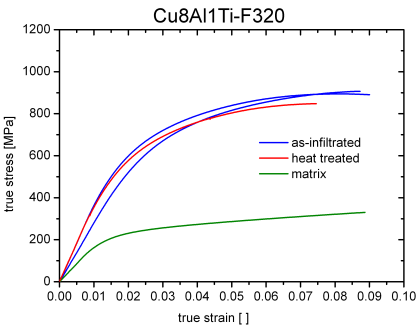

(f)

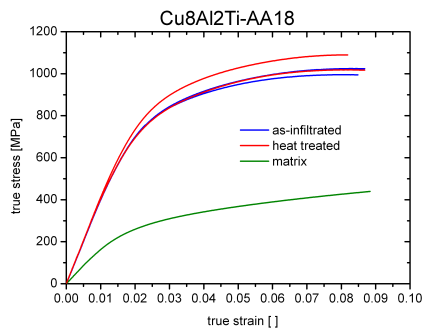

(g)

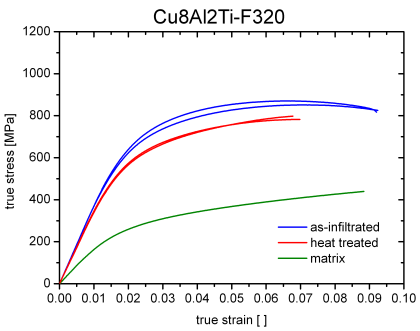

(h)

Figure 16: Compression curves of infiltrated composites: (a) Cu8Al-AA18 (b) Cu8Al-F320 (c) Cu8Al0.2Ti-AA18 (d) Cu8Al0.2Ti-F320 (e) Cu8Al1Ti-AA18 (f) Cu8Al1Ti-F320 (g) Cu8Al2Ti-AA18 (h) Cu8Al2Ti-F320

is in contact with alumina in infiltration (≈3 min) versus the time taken for brazing or wetting experiments (15 min or more). The titanium-rich layer found here is distinctly thinner than in any of the brazed layers; it is so thin (5 to 10 nm) that we could not ascertain here whether it is a distinct new interfacial phase or just a thin Ti-rich film, or complexion, along the interface separating the primary copper-rich phase from alumina. The data obtained by the EDX line-scan shown in Fig.8b show a sharp Ti gradient, suggesting the presence of a distinct boundary as would be the case for a Ti-rich phase. Several binary titanium oxides are stable at the infiltration temperature of 1150°C: β-TiO, β-Ti_2O_3 and several other oxides [53], but our data do not allow a final conclusion on the question.

The apparently lower reactivity between Ti in the metal and alumina that is observed here compared to literature data on similar systems can have several possible origins. One is the potential role of differences in oxygen chemical activity from one experiment to the other. Another is the fact that aluminum will lower the titanium chemical activity in copper, because it can form stable compounds with titanium, such as titanium aluminides or the $AlCu_2Ti$ intermetallic observed here. This effect parallels what happens when Ni is added to a Ti-containing CuAg-alloy, a system documented in Ref. [51]: the interface then shows a single roughly 100 nm thick titanium-enriched layer. This change in interface structure was explained the fact that strong Ni-Ti interactions within the melt (nickel has a strong chemical affinity for titanium) decrease the Ti chemical activity causing in turn a drastic decrease in the interfacial reactivity of titanium and a suppression of mixed oxide formation in that system [51]. Unlike nickel, however, the affinity between titanium and aluminum is apparently not sufficient to suppress here the formation of a titanium-containing mixed oxide. A third factor is time: molten metal/ceramic contact times are far shorter in making the present composites than they are in brazing or sessile drop wetting drop experiments.

The mechanical strength of the interface in brazed samples has been attributed to the presence of $Ti_3(Cu,Al)_3O$ [36, 51, 52]. Our results suggest otherwise for infiltrated composites: an alloy of low Ti activity, which forms only a nanometric Ti-rich film between the metal and the ceramic, is optimal. Here, more titanium in the matrix has a negative effect: it degrades the interfacial strength because it increases the volume fraction of brittle $Ti_3(CuAl)_3O$, Fig.14. This difference can have several causes; worthy of mention in this regard is the fact that in brazing or wetting experiments, an interface can only be mechanically strong if wetting is sufficient to create a sound bond. Present composites are produced by pressure infiltration so that, here, the bond integrity is not tributary to good wetting (good wetting and strong bonding do not always come together: the Al-Al_2O_3-system gives a good example of moderate wetting associated with strong adhesion, e.g. Ref. [50, 54]).

A far more extensive transmission electron microscopic characterization of the thin titanium-rich layer in Fig.8 would be needed to determine its precise thickness, composition and atomic structure. Given how thin it is (at most 10 nm, Fig.8) and given the fact that there is little overlap between the oxygen-rich and the titanium-rich regions in Fig.8 (making it unlikely that we have here a nanometric titanium oxide layer akin to those reported

in Refs. [31, 55]), the interface between Ti-containing Cu8Al and alumina is likely to be a nanometric Ti-rich interfacial film associated with a discontinuous jump in Ti adsorption, designated using the word complexion in recent terminology [56–62], and similar to the very thin Ti-rich film that forms along the interface between alumina and Au-Ti alloys [63]. Mechanical properties of the present composites are interesting in this light: they show with clarity that the Ti-rich Cu8Al/alumina interface complexion that may have formed here is one that leads to a much stronger interface between Cu8Al and alumina.

4.2. Mechanical properties

In all mechanical tests AA18 composites are found to be superior to F320 composites, regardless of the matrix composition. Several factors explain this:

(i) the F320 Al_2O_3 particles are intrinsically weaker. Virgin particles contain cracks, as shown in Fig.1b, which arise due to their production process (comminution). These cracks can explain why hardness, Young's modulus, tensile strength, elongation, and compression yield strength are all lower for F320 than for AA18 composites. This parallels what has been documented for aluminum matrix composites [54, 64–67];

(ii) the presence of β-Al_2O_3 might also play a role,

(iii) as might the angular form of the F320 Al_2O_3 particles, which increases stress concentration and tri-axiality in comparison with more rounded AA18 Al_2O_3 particles [68, 69].

The influence of the heat treatment on the mechanical properties is minor in all composites except for those with a matrix of Cu8Al. In Cu8Al-AA18, the applied heat treatment leads to a slight increase in tensile elongation, perhaps due to relaxation of thermal stresses developed during the production process (see below). For Cu8Al-F320 composites, however, the heat treatment reduces the tensile elongation while it increases the UTS by a factor of almost two. In compression we also observe that $\sigma_{0.2\%}$ in Cu8Al composites increases after the heat treatment. We do not know the reason for this change, but believe it might be related to a thermally activated process, e.g diffusion of the Na-impurities to the interface or relaxation of thermal stresses. As the (poor) mechanical properties of these particular composites are not of great interest, we did not investigate in detail this phenomenon.

The matrix alloy composition strongly influences the mechanical properties of the infiltrated composites. Addition of titanium leads in all cases to an improvement of the mechanical properties; however, the quantity of Ti added does not influence all measured properties in the same way, e.g. hardness increases with increasing Ti content, while the UTS does not. The increase in hardness with Ti content of both the unreinforced matrix alloys and the composites is explained by the increasing volume fraction of second phases: $AlCu_2Ti$ in the matrix alloys and $Ti_3(Cu,Al)_3O$ in the composites.

The same tendency is observed for Young's modulus of F320 composites: an increasing Ti content leads to increasing Young's modulus. The Young's modulus of Cu8Al-F320 is very low for a composite containing 56vol% Al_2O_3 particles: it is well below what is predicted by the Mori-Tanaka approximation for Young's

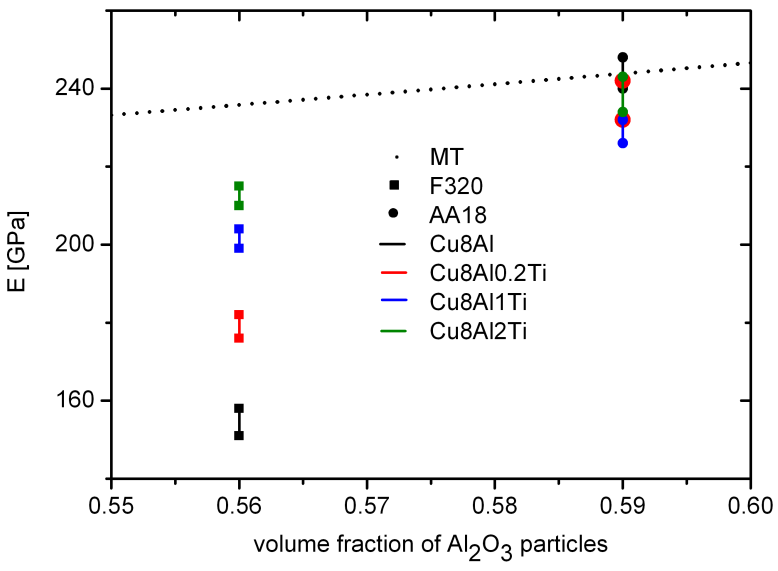

Figure 17: Young's modulus as a function of alumina volume fraction for infiltrated composites compared to Mori-Tanaka prediction

modulus, Fig.17 (values taken for calculation are: $G_{Al_2O_3}$= 164 GPa, $K_{Al_2O_3}$= 238 GPa, G_{Cu}= 48 GPa, K_{Cu}= 140 GPa, ν_{Cu}=0.34 [44, 45]).

With increasing Ti content the Young's modulus of the F320 composites increases and approaches the value predicted by Mori-Tanaka approximation (which coincides with the lower Hashin-Shtrikman bound), but does not reach it. Cu8Al-AA18 has a modulus that equals the Mori-Tanaka prediction, even though the interface between Cu8Al and AA18 is not very strong, as can be seen in tensile tests, Fig.10a. The reason for the low Young's modulus of Cu8Al-F320 is therefore probably not the mechanically weak interface between Cu8Al and F320, but rather an intrinsically lower modulus of the F320 powder, which could be explained by (i) the internal cracks that are present in these particles, see. Fig.1b and/or (ii) the β-Al_2O_3 present in the F320 alumina (although literature data vary between 160 GPa [70] and 210 GPa [71], β-Al_2O_3 has a lower Young's modulus than α-Al_2O_3). This interpretation is confirmed by the Young's moduli of the other F320 composites, which also remain below the Mori-Tanaka model despite the strong interfaces.

The increase in Young's modulus of F320 composites with increasing Ti content can be explained by increasing coverage of the F320 particles with $Ti_3(Cu,Al)_3O$: these might heal surface cracks (Fig.4b suggests this with the visible presence of metal-rich zones inside F320 particles). As the Young's modulus of $Ti_3(Cu,Al)_3O$ is $\approx$180 GPa [72], i.e. below that of α-alumina (400 GPa), one can also explain why the Young's modulus of the AA18 composites decreases slightly with increasing volume content of $Ti_3(Cu,Al)_3O$.

Data for $\sigma_{0.2\%}$ from compression tests confirm hardness and tensile data: adding Ti to the matrix hardens the

composites; however, by far the most important increase is already reached with 0.2wt%Ti.

The UTS and tensile elongation reach a peak with Cu8Al0.2Ti matrices: the interface is mechanically improved by Ti in (small) quantities sufficient to form a thin Ti-rich layer such as can be seen in Fig.8. Properties are then degraded if more titanium is added, since this leads to decoration of the interface with weaker $Ti_3(Cu,Al)_3O$. Fracture surfaces confirm that, unlike what is found for Ti-free Cu8Al, the interface between Cu8Al0.2Ti and Al_2O_3 is strong, Figs.11 and 12. Fracture surfaces become more complex with Cu8Al1Ti and Cu8Al2Ti matrices: the interface phase $Ti_3(Cu,Al)_3O$ is now also fractured, as evident in Figs.13, 14, alongside broken Al_2O_3 particles.

Cyclic unloading/reloading tensile tests show that F320 composites damage slightly faster than do AA18 composites, albeit not dramatically so: $dD_E/d\epsilon$=18 and 23 for AA18 and F320, respectively. This is also documented in Ref.[64], where D_E was measured in pure Al matrix composites of the same two Al_2O_3 particle types. The pure Al matrix composites can be deformed further than the alloyed Cu matrix composites used in this work, and past a certain plastic deformation (not reached here) the damage parameter is no longer a linear function of the plastic strain. In the initial low-strain region, D_E can be approximated by a straight line of slope $dD_E/d\epsilon = 5$ for AA18 [73] and 6 for F320 [64] in pure Al. Damage accumulation rates in pure Al are thus much lower than for the same particles in alloyed Cu matrices.

This is confirmed in Ref.[65], where the damage evolution of AA18 and F320 particles is measured in three different matrices: pure Al, Al2wt%Cu and Al4.5wt%Cu. For all composites it was found that

(i) the damage evolution rate is higher for the angular particles ($dD_E/d\epsilon = 8$ in pure Al, 10 in Al2wt%Cu and 20 in Al4.5wt%Cu) than in polygonal AA18 particles ($dD_E/d\epsilon = 5$ in pure Al, 4 in Al2wt%Cu and 7 in Al4.5wt%Cu) and

(ii) with increasing matrix strength, $dD_E/d\epsilon$ increases (an exception is for AA18 particles in Al2wt%Cu, but the data show a discontinuous jump after 1% strain and are thus questionable).

Still, even with alloyed Al matrices the damage accumulation rate remains less than for the present Cu8Al-Ti composites.This is likely caused by the higher flow stress and perhaps also by the lower propensity for cross-slip in the matrix of the present copper matrix composites (see below).

On comparing tensile and compressive stress-strain curves of the composites (Figs.10 and 16 respectively) one notes that these flow at higher stress in compression than in tension. One cause for this difference is internal damage by particle fracture, which is likely to decrease the flow stress in tension more than in compression.

The effect can be quantified using the simplified analytical approach of Ref. [74]. In that work a variational model was adapted to predict in relatively simple terms the flow curve of isotropic composites made of a power-law metal matrix reinforced with rigid particles. The influence of particle cracking was accounted for by assuming that cracked particles can be replaced, in the model, by as much matrix material (an assumption justified by micromechanical calculations of cracked equiaxed particles in an elastic matrix [74]). Making this

assumption and using the Mori-Tanaka expression for Young's modulus, the volume fraction, V_{r2}, of particles cracked within the composite can then be deduced, as a function of tensile strain ϵ, from the measured evolution of the composite modulus (given in Fig.15 as D_E versus ϵ). From this, using Eq. (1) of Ref. [74]:

$$E_C = \frac{9K_C G_C}{G_C + 3K_C} \tag{2}$$

where

$$K_C = K_m + \frac{(1 - V_m - V_{r2})(K_r - K_m)(3K_m + 4G_m)}{3(V_m + V_{r2})(K_r - K_m) + 3K_m + 4G_m} \tag{3}$$

$$G_C = G_m \frac{(1 - V_m - V_{r2})(G_r - G_m)G_m}{\beta_m(V_m + V_{r2})(G_r - G_m) + G_m} \tag{4}$$

$$\beta_m = \frac{6}{5}\frac{K_m + 2G_m}{3K_m + 4G_m}. \tag{5}$$

V_{r2} can be deduced as a function of ϵ from the tensile curve and measurements of damage parameter D_E. E_C is the Young's modulus of the composite, K_C, G_C, K_m, G_m, K_r and G_r are the bulk and shear moduli of the composite, the matrix and the reinforcement, respectively, while V_m is the initial volume fraction of matrix phase. Using the variational estimate with the assumption that a cracked particle behaves roughly as an equivalent volume of matrix, the relative reduced plastic flow stress Σ/Σ_0 where Σ_0 is the undamaged composite flow stress, can be calculated as a function of V_m, V_{r2} and the hardening exponent n, Eq. (12) of Ref. [74]:

$$\frac{\Sigma}{\Sigma_0} = \left(\frac{5 - 3V_m - 3V_{r2}}{5 - 3V_m}\right)^{\frac{1+n}{2}} \cdot \left(\frac{V_m}{V_m + V_{r2}}\right)^n. \tag{6}$$

The hardening exponent n is found to be quite similar for the matrix (0.19 measured from the onset of plastic deformation up to 1% plastic strain) and the composite (0.17 measured from compression curves from 1% up to 2.5% plastic deformation and 0.19 from the tensile curves from 0.2% up to fracture) - as should be, according to theory. We take $n = 0.19$ in estimating the flow curve of the composite in the absence of internal damage; the result is given in Fig.18a for Cu8Al0.2Ti-AA18. As seen, damage in form of broken particles can explain only a small part of the difference between measured tensile and compressive composite flow curves.

Two alternative explanations offer themselves to explain the remaining difference between the compressive and the "effective" (calculated, damage-free) tensile flow curve of the composite, namely (i) another form of internal damage and (ii) internal stresses. Additional damage is present, in the form of matrix voiding, Fig.19; however, its extent is very limited and it is not likely to account for a 100 MPa difference in flow stress of the composite. The second mechanism, namely the presence of internal stresses in the composite, is thus to be retained as the more likely cause for the difference between the two.

High internal stresses are known to arise in metal matrix composites due to the difference in the coefficient of thermal expansion between the matrix (α_m=17·10^{-6}1/K) and the reinforcement (α_r=8·10^{-6}1/K) [45]. Differential contraction during cool-down from processing temperatures are well known to cause, in systems where these can not be compensated by matrix recovery, a build-up of internal stresses, the average trace of which is

compressive in the particles, tensile in the matrix, and hence likely to cause the composite yield stress to be lower in tension than in compression - as observed here.

A second consequence of matrix/particle differential thermal contraction is matrix hardening, a result of thermal stress relief by dislocation punching [75]. To estimate the extent of this effect in the present composites, we make use of the simplified metal matrix composite flow curve prediction scheme of Mueller et al. [76]. For ease of processing and because it agrees with data for AA18 particle composites, Fig.17, we use the simple Mori-Tanaka model to describe composite elastic properties. On this basis, one can then estimate the ratio of composite strength coefficient C to matrix strength coefficient c in their (same exponent n) power-law flow curve. This is given as:

$$\frac{C}{c} = \frac{\left(\frac{3}{2}V_r + 1\right)^{(n+1)/2}}{(1 - V_r)^n} \tag{7}$$

with V_r = 1 - V_m the initial volume fraction of reinforcement [74]. Two thus back-calculated *in-situ* matrix flow curves are shown in Fig.18b, one from a composite compressive curve, the other from a composite effective tensile curve. The measured compressive curve from a sample of the unreinforced matrix is given as well. As seen, both *in-situ* matrix curves show much higher flow stresses than the unreinforced Cu8Al0.2Ti matrix. The particles thus harden the metal significantly: the *in-situ* flow stress is some 300 MPa higher than in the as-cast, unreinforced condition, Fig.18b. The difference between tension and compression additionally suggests an average matrix internal tensile stress on the order of 50 MPa.

A main cause for matrix hardening in composites is differential thermal contraction between matrix and particles during cooldown of the composites from processing temperatures. We use a simple model of geometrically necessary prismatic loop punching (Eq. (7) of Ref.[77]):

$$\rho_G = \frac{12V_r(\alpha_r - \alpha_m)\Delta T}{(1 - V_r)\, bD} \tag{8}$$

and the Taylor-formula for work hardening [78]

$$\Delta\tau = KG_m b\sqrt{\rho_G} \tag{9}$$

where D is the average particle diameter, b=2.54·10^{-10} m is the Burgers vector of Cu [78], $\Delta\tau$ is the increase in shear stress due to an increased number of dislocations and K a constant taken as 0.4 [79]. The calculated value of ρ_G is then obtained as 4·10^{13} per m^2 giving $\Delta\tau$=29 MPa, corresponding to a difference in tensile flow stress of roughly twice this amount.

This is half an order of magnitude less than the difference found in Fig.18b. For comparison, in pure aluminum this simple model was found to give a reasonable prediction of dislocational matrix hardening caused by matrix/ceramic differential contraction. Perhaps this difference between aluminum and Cu8Al02Ti is caused by the difference in stacking fault energy and therefore in ease of cross-slip between the two metals.

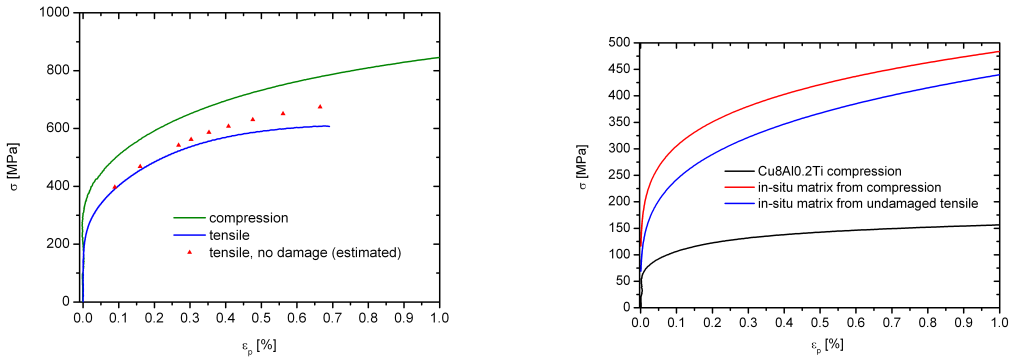

(a) (b)

Figure 18: Stress-strain curves; (a) tensile and compressive curves of Cu8Al0.2Ti-AA18 together with calculated undamaged points of tensile curve (b) *in-situ* matrix stress-strain curves for Cu8Al0.2Ti-AA18 compared to measured compressive curve of the unreinforced matrix

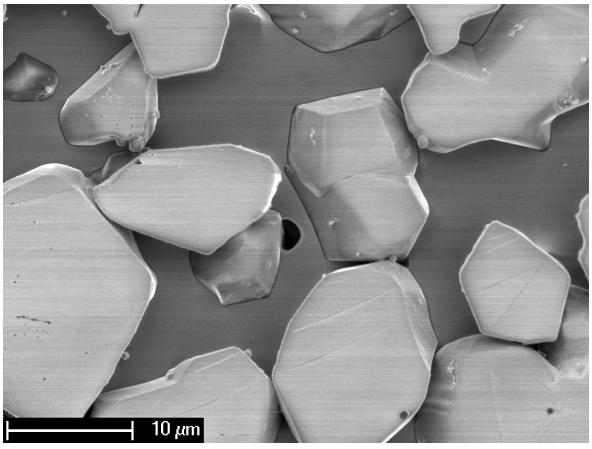

Figure 19: SEM image of tensile specimen of Cu8Al0.2Ti-AA18 polished and electrolytically etched,loading direction perpendicular to the scale bar

5. CONCLUSION

- The addition of Ti to the matrix of infiltrated particulate Cu-8Al matrix composites containing 56 to 59 vol% Al_2O_3 particles increases their hardness, tensile strength, compressive strength and ductility in comparison to similar composites devoid of titanium.

- The optimal Ti content found here is 0.2wt%Ti, i.e. the lowest explored in the present experiments. With this concentration, the majority of the interface between the primary copper-aluminum matrix and the alumina particles is a very thin (5-10 nm) titanium-rich layer. This layer is likely to be an interfacial complexion associated with a discontinuous jump in Ti adsorption; our results suggest that this particular complexion produces a significantly increased mechanical strength for the interface between the copper-aluminum matrix and alumina.

- A further increase in the Ti-content leads to formation of a second interface phase, $Ti_3(Cu,Al)_3O$; mechanical and metallographic data show that this phase is brittle and degrades the interface strength.

- Angular comminuted alumina particles lead to inferior mechanical properties compared to polygonal vapour-grown alumina particles, independent of the matrix composition, as was found in earlier work on similar Al-Al_2O_3 composites. Data suggest that increasing the matrix Ti-content may partly heal the particles; however, the effect on composite strength is slight and overcompensated by interfacial weakening caused by the presence of $Ti_3(Cu,Al)_3O$.

- Composites with a Cu8Al0.2Ti matrix reinforced with polygonal Al_2O_3 particles have the best mechanical properties, namely a Young's modulus near 235 GPa, a density of 5.5 g/cm^3, a tensile strength and elongation of 600 MPa and 1% respectively, together with a compressive strength near 1100 MPa reached at 9% strain.

- Comparison with Al-based composites reinforced with the same particles at similar volume fractions shows that the *in-situ* matrix flow stress is increased more drastically, but also the tensile elongation is smaller, when the matrix is of a copper alloy. Analysis of the difference between the two matrices suggests that the known difference in stacking fault energy, and in the ensuing ease of cross-slip, between the two metals increases strongly dislocational hardening effects in copper-based matrix composites compared with aluminum.

Acknowledgements

We gratefully acknowledge help from Dr. K Schenk of IBSP, EPFL who performed Rietveld refinement to determine the exact lattice parameter of $Ti_3(Cu,Al)_3O$ and from Dr. M. Cantoni, CIME, EPFL for conducting FIB and TEM experiments. This work was funded by the KTI/CTI Förderagentur für Innovation through CTI project 9026.1 PFIW-IW in collaboration with the company Swissmetal (Dornach, Switzerland). We finally gratefully acknowledge many stimulating discussions of this work with colleagues at Swissmetal, particularly Mr. Jean-Pierre Tardent, Dr. Claudio Penna, Dr. Florian Dalla Torre, and Dr. Nathanael Dewobroto, with Professor W. Craig Carter of the Massachusetts Institute of Technology in Cambridge, MA, USA, and with Professor Wayne D Kaplan of the Technion, in Haifa, Israel.

BIBLIOGRAPHY

[1] Biselli, C., Morris, D., Randall, N.. Mechanical alloying of high-strength copper-alloys containing TiB_2 and Al_2O_3 dispersoid particles. Scripta Mater 1994;30(10):1327–1332.

[2] Chrysanthou, A., Erbaccio, G.. Production of copper-matrix composites by in situ processing. J Mater Sci 1995;30(24):6339–6344.

[3] Lee, J., Jung, J., Lee, E., Park, W., Ahn, S., Kim, N.. Microstructure and properties of titanium boride dispersed Cu alloys fabricated by spray forming. Mater Sci Eng, A 2000;277(1-2):274–283.

[4] Kim, J., Kwon, Y., Lomovsky, O., Korchagin, M., Mali, V., Dudina, D.. A synthetic route for metal-ceramic interpenetrating phase composites. Mater Lett 2006;60(29-30):3723–3726.

[5] Martinez Pacheco, M., Bouma, R., Katgerman, L.. Combustion synthesis of TiB_2-based cermets: modeling and experimental results. Appl Phys A 2008;90:159–163.

[6] Chen, G.Q., Xiu, Z.Y., Meng, S.H., Wu, G.H., Zhu, D.Z.. Fabrication and thermo-physical properties of TiB_{2p}/Cu composites for electronic packaging applications. Transactions of Nonferrous Metals Society of China 2009;19(2):448–452.

[7] Winzer, J., Weiler, L., Pouquet, J., Roedel, J.. Wear behaviour of interpenetrating alumina-copper composites. Wear 2011;271(11-12):2845–2851.

[8] Travitzky, N., Shlayen, A.. Microstructure and mechanical properties of Al_2O_3/Cu-O composites fabricated by pressureless infiltration technique. Mater Sci Eng, A 1998;244(2):154–160.

[9] Jena, P., Brocchi, E., Motta, M.. In-situ formation of Cu-Al_2O_3 nano-scale composites by chemical routes and studies on their microstructures. Mater Sci Eng, A 2001;313(1-2):180–186.

[10] Simchi, H., Simchi, A.. Tensile and fatigue fracture of nanometric alumina reinforced copper with bimodal grain size distribution. Mater Sci Eng, A 2009;507(1-2):200–206.

[11] Nachum, S., Fleck, N., Ashby, M., Colella, A., Matteazzi, P.. The microstructural basis for the mechanical properties and electrical resistivity of nanocrystalline Cu-Al_2O_3. Mater Sci Eng, A 2010;527(20):5065–5071.

[12] Weber, L., Tavangar, R.. On the influence of active element content on the thermal conductivity and thermal expansion of Cu-X (X = Cr, B) diamond composites. Scripta Mater 2007;57(11):988–991.

[13] Schubert, T., Trindade, B., Weissgarber, T., Kieback, B.. Interfacial design of Cu-based composites prepared by powder metallurgy for heat sink applications. Mater Sci Eng, A 2008;475(1-2):39–44.

[14] Wang, W., Takao, Y., Matsubara, T.. Tensile strength and fracture toughness of C/C and metal infiltrated composites Si-C/C and Cu-C/C. Composites Part A 2008;39(2):231–242.

[15] Liu, L., Tang, Y., Zhao, H., Zhu, J., Hu, W.. Fabrication and properties of short carbon fibers reinforced copper matrix composites. J Mater Sci 2008;43(3):974–979.

[16] Vetterli, M., Tavangar, R., Weber, L., Kelly, A.. Influence of the elastic properties of the phases on the coefficient of thermal expansion of a metal matrix composite. Scripta Mater 2011;64(2):153–156.

[17] Maruyama, T., Onose, S.. Fabrication and thermal conductivity of boron carbide copper cermet. J Nucl Sci Technol 1999;36(4):380–385.

[18] Zarrinfar, N., Kennedy, A., Shipway, P.. Reaction synthesis of Cu-TiC_x master-alloys for the production of copper-based composites. Scripta Mater 2004;50(7):949–952.

[19] Schubert, T., Brendel, A., Schmid, K., Koeck, T., Ciupinski, L., Zielinski, W., et al. Interfacial design of Cu/SiC composites prepared by powder metallurgy for heat sink applications. Composites Part A 2007;38(12):2398–2403.

[20] Zhang, L., Qu, X., He, X., Duan, B., Ren, S., Qin, M.. Thermo-physical and mechanical properties of high volume fraction SiC_p/Cu composites prepared by pressureless infiltration. Mater Sci Eng, A 2008;489(1-2):285–293.

[21] Rathod, S., Modi, O., Prasad, B., Chrysanthou, A., Vallauri, D., Deshmukh, V., et al. Cast in situ Cu-TiC composites: Synthesis by SHS route and characterization. Mater Sci Eng, A 2009;502(1-2):91–98.

[22] Krüger, C., Laporte, V., Mortensen, A.. Copper metal matrix composites: processing and mechanical properties of ceramic and carbon nanotube reinforced systems : under review;.

[23] Mortensen, A.. Melt Infiltration of Metal Matrix Composite, Chapter 3.20. Comprehensive Composite Materials, Vol. 3: Metal Matrix Composites; Oxford UK: Pergamon; 2000.

[24] Naidich, J.. The wettability of solids by liquid metals. Progress in surface and membrane science 1981;14:353–484.

[25] Eustathopoulos, N., Nicholas, M., Drevet, B.. Wettablity at High Temperatures; vol. 3 of *Pergamon Material Series*. Amsterdam: Pergamon; 1999.

[26] Saiz, E., Cannon, R., Tomsia, A.. High-temperature wetting and the work of adhesion in metal/oxide systems. Annu Rev Mater Res 2008;38:197–226.

[27] Kritsalis, P., Li, J., Coudurier, L., Eustathopoulos, N.. Role of clusters on the wettability and work of adhesion of the Cu-Cr/Al_2O_3 system. J Mater Sci Lett 1990;9(11):1332–1335.

[28] Kritsalis, P., Coudurier, L., Eustathopoulos, N.. Contribution to the study of reactive wetting in the CuTi/Al_2O_3 system. J Mater Sci 1991;26(12):3400–3408.

[29] Naidich, Y., Zhuravlev, V., Chuprina, V., Strashinskaya, L.. Adhesion, wetting, and formation of intermediate phases in systems composed of a titanium-containing melt and an oxide. Soviet Powder Metallurgy and Metal Ceramics 1973;12(11):895–899.

[30] Loehman, R., Tomsia, A.. Reactions of Ti and Zr with AlN and Al_2O_3. Acta Metall et Mat 1992;40:S75–S83.

[31] Derby, B., Webster, J.. Neutron reflection studies of the composition of interfaces between titanium containing active braze alloys and sapphire. Trans JWRI 2001;30(Special issue):233–238.

[32] Carim, A.. Convergent-beam electron-diffraction fingerprinting of M_6X phases at brazed ceramic joints. Scripta Metall et Mater 1991;25(1):51–54.

[33] Derby, B., Xiao, P., Webster, J.. Neutron reflection studies of titanium segregation to metal-ceramic interfaces. Physica B 1998;248:304–309.

[34] Vianco, P., Stephens, J., Hlava, P., Walker, C.. Titanium scavenging in Ag-Cu-Ti active braze joints. Welding Journal 2003;82(10):268S–277S.

[35] Voytovych, R., Ljungberg, L., Eustathopoulos, N.. The role of adsorption and reaction in wetting in the CuAg-Ti/alumina system. Scripta Mater 2004;51(5):431–435.

[36] Voytovych, R., Robaut, F., Eustathopoulos, N.. The relation between wetting and-interfacial chemistry in the CuAgTi/alumina system. Acta Mater 2006;54(8):2205–2214.

[37] Kozlova, O., Voytovych, R., Eustathopoulos, N.. Initial stages of wetting of alumina by reactive CuAgTi alloys. Scripta Mater 2011;65(1):13–16.

[38] Nicholas, M., Valentine, T., Waite, M.. The wetting of alumina by copper alloyed with titanium and other elements. J Mater Sci 1980;15(9):2197–2206.

[39] Meier, A., Chidambaram, P., Edwards, G.. Generation of isothermal spreading data and interfacial energy data for liquid reactive metals on ceramic substrates - the copper-titanium alumina system. J Mater Sci 1995;30(15):3791–3798.

[40] Nicholas, M., editor. Joining of ceramics. Advanced ceramic reviews; London: Chapman and Hall; 1990.

[41] Fujiwara, S., Tamura, Y., Maki, H., Azuma, N., Takeuchi, Y.. Development of new high-purity alumina. R&D Report "Sumitomo Kagaku" 2007;1.

[42] Bahraini, M., Molina, J., Kida, M., Weber, L., Narciso, J., Mortensen, A.. Measuring and tailoring capillary forces during liquid metal infiltration. Curr Opin Solid State Mater Sci 2005;9(4-5):196–201.

[43] ASTM E 1876-99; Standard Test method for Dynamic Young's Modulus, Shear Modulus and Poisson's Ratio by Impulse Excitation of Vibration. West Conshohocken, PA: ASTM International; 1999.

[44] Simmons, G., Wang, H.. Single crystal elastic constants and calculated aggregate properties. Second ed.; Cambridge, Massachusetts, USA: M.I.T. Press; 1971.

[45] Gale, W., Totemeier, T., editors. Smithells Metals reference book. 8th ed.; Amsterdam; Boston: Elsevier Butterworth-Heinemann; 2004.

[46] ASTM E8/E8M-09; Standard Test Methods for Tension Testing of Metallic Materials. West Conshohocken, PA: ASTM International; 2009.

[47] Dyson, D., Johnson, W.. Identification of beta-alumina type phases. Transactions and Journal of the British Ceramic Society 1973;72(2):49–55.

[48] Krüger, C.. Ph.D. thesis; EPFL; 2012. Nr. 5422.

[49] Kelkar, G., Carim, A.. Al solubility in M_6X compounds in the Ti-Cu-O system. Mater Lett 1995;23(4-6):231–235.

[50] Kouzeli, M., Weber, L., Marchi, S., Mortensen, A.. Quantification of microdamage phenomena during tensile straining of high volume fraction particle reinforced aluminium. Acta Mater 2001;49(3):497–505.

[51] Valette, C., Devismes, M., Voytovych, R., Eustathopoulos, N.. Interfacial reactions in alumina/CuAgTi braze/CuNi system. Scripta Mater 2005;52(1):1–6.

[52] Kozlova, O., Braccini, M., Voytovych, R., Eustathopoulos, N., Martinetti, P., Devismes, M.. Brazing copper to alumina using reactive CuAgTi alloys. Acta Mater 2010;58(4):1252–1260.

[53] Massalski, T.. Binary Alloy Phase Diagrams; vol. 1. second ed.; Ohio, US: ASM International; 1990.

[54] Miserez, A., Rossoll, A., Mortensen, A.. Fracture of aluminium reinforced with densely packed ceramic particles: link between the local and the total work of fracture. Acta Mater 2004;52(5):1337–1351.

[55] Gremillard, L., Saiz, E., Radmilovic, V., Tomsia, A.. Role of titanium on the reactive spreading of lead-free solders on alumina. J Mater Res 2006;21:3222–3233.

[56] Scheu, C., Dehm, G., Kaplan, W.. Equilibrium amorphous silicon-calcium-oxygen films at interfaces in copper-alumina composites prepared by melt infiltration. J Am Ceram Soc 2001;84(3):623–630.

[57] Avishai, A., Scheu, C., Kaplan, W.. Intergranular films at metal-ceramic interfaces: Part i - interface structure and chemistry. Acta Mater 2005;53(5):1559.

[58] Avishai, A., Kaplan, W.. Intergranular films at metal-ceramic interfaces: Part ii - calculation of hamaker coefficients. Acta Mater 2005;53(5):1571.

[59] Tang, M., Carter, W., Cannon, R.. Grain boundary order-disorder transitions. J Mater Sci 2006;41(23):7691–7695.

[60] Tang, M., Carter, W., Cannon, R.. Grain boundary transitions in binary alloys. Phys Rev Lett 2006;97(7):075502.

[61] Kaplan, W., Chatain, D., Wynblatt, P., Carter, W.. A review of wetting versus adsorption, complexions, and related phenomena: the rosetta stone of wetting. J Mater Sci 2013;48(17):5681–5717.

[62] Baram, M., Kaplan, W.. Intergranular films at au-sapphire interfaces. J Mater Sci 2006;41(23):7775–7784.

[63] Nussbaum, E., Meltzman, H., Kaplan, W.. Equilibrium segregation of ti to au-sapphire interfaces. J Mater Sci 2012;47(4):1647–1654.

[64] Kouzeli, M., Weber, L., San Marchi, C., Mortensen, A.. Influence of damage on the tensile behaviour of pure aluminium reinforced with > 40 vol. pct alumina particles. Acta Mater 2001;49(18):3699–3709.

[65] Mueller, R.. Ph.D. thesis; EPFL; 2007.

[66] Miserez, A., Müller, R., Rossoll, A., Weber, L., Mortensen, A.. Particle reinforced metals of high ceramic content. Mater Sci Eng, A 2004;387-389:822–831.

[67] Miserez, A., Mortensen, A.. Fracture of aluminum reinforced with densely-packed ceramic particles: Influence of matrix hardening. Acta Mater 2004;52(18):5331–5345.

[68] Qin, S., Chen, C., Zhang, G., Wang, W., Wang, Z.. The effect of particle shape on ductility of SiC_p reinforced 6061 Al matrix composites. Mater Sci Eng, A 1999;272(2):363–370.

[69] Chen, C., Qin, S., Li, S., Wen, J.. Finite element analysis about effects of particle morphology on mechanical response of composites. Mater Sci Eng, A 2000;278(1-2):96–105.

[70] Stevens, R.. Strength and fracture mechanisms in beta-alumina. J Mater Sci 1974;9(6):934–940.

[71] Tan, S., May, G.. The dependence of the fracture stress of beta-alumina on microstructural defects. J Mater Sci 1977;12(5):1058–1061.

[72] Kelkar, G., Carim, A.. Synthesis, properties, and ternary phase-stability of M_6X compounds in the Ti-Cu-O system. J Am Ceram Soc 1993;76(7):1815–1820.

[73] Kouzeli, M.. Ph.D. thesis; EPFL; 2001.

[74] Mueller, R., Rossoll, A., Weber, L., Bourke, M., Dunand, D., Mortensen, A.. Tensile flow stress of ceramic particle-reinforced metal in the presence of particle cracking. Acta Mater 2008;56(16):4402–4416.

[75] Calhoun, R., Dunand, D.. Dislocations in Metal Matrix Composites, Chapter 3.02. Comprehensive Composite Materials, Vol. 3: Metal Matrix Composites; Oxford UK: Pergamon; 2000.

[76] Mueller, R., Mortensen, A.. Simplified prediction of the monotonic uniaxial stress-strain curve of non-linear particulate composites. Acta Mater 2006;54(8):2145–2155.

[77] Kouzeli, M., Mortensen, A.. Size dependent strengthening in particle reinforced aluminium. Acta Mater 2002;50(1):39–51.

[78] Meyers, M., Chawla, K.. Mechanical Behavior of Materials. second ed.; Cambridge: Cambridge University Press; 2009.

[79] Mughrabi, H., editor. Plastic deformation and fracture of materials; vol. 6 of *MATERIALS SCIENCE AND TECHNOLOGY: a comprehensive treatment*. Weinheim: Wiley-VCH; 2005.